Constructing the Universe with Clusters of Galaxies, IAP 2000 meeting, Paris (France) July 2000
Florence Durret & Daniel Gerbal eds.

THE EUV EXCESS EMISSION OF THE VIRGO AND A1795 CLUSTERS - RE-OBSERVATION WITH IN-SITU BACKGROUND MEASUREMENTS

Richard Lieu[1], Massimiliano Bonamente[2], Jonathan P.D. Mittaz[3]
1) Department of Physics, University of Alabama, Huntsville, AL 35899, U.S.A.
2) Osservatorio Astrofisico di Catania, Via S. Sofia 78, I-95125 Catania, Italy
3) Mullard Space Science Laboratory, UCL, Holmbury St. Mary, Dorking, Surrey, RH5 6NT, U.K.

The Virgo and A1795 clusters of galaxies were re-observed by EUVE with *in situ* background measurements by pointing at small offsets. Earlier, a similar re-observational strategy applied to the cluster A2199 revealed that the background radial profile was consistent with a flat distribution, and therefore the original method of extracting cluster EUV signals by the subtraction of an aymptotically determined background was valid. It is shown here that the same conclusions hold for the current sample. In particular, for A1795, the *in situ* background was observed with equal exposure as that for the cluster (each 78 ksec), no tangible inner enhancement of the background profile (which may mimic cluster emission) is apparent. A model of the background was obtained from its known properties and the *in situ* measurements. The subtracted cluster fluxes remain in agreement with those reported in our discovery papers. They are also consistent with results from the most conservative procedure of direct point-to-point subtraction of the *in situ* background and proper error propagation, which still preserves the existence of the EUV excess and its rising radial trend. We present evidence which argues against the soft excess as due to peculiarities in the line-of-sight Galactic absorption. The data appear to favor a thermal origin of the emission.

1 Introduction

Clusters of galaxies are sources which emit EUV and soft X–ray radiation ($\sim$ 0.1– 0.4 keV) substantially in excess of that expected from the hot intra–cluster medium (ICM) at X–ray temperatures (a few keV). The *Extreme Ultraviolet Explorer* mission (Bowyer and Malina 1991) was pivotal to the discovery of this phenomenon, as it opened a unique window to the EUV sky with the Deep Survey (DS) Lex/B filter ($\sim$ 65–190 eV, hereafter the EUV band). Cluster soft–excess (CSE) emission was reported for the Virgo (Lieu et al. 1996a), Coma (Lieu et al. 1996b), A1795 (Mittaz, Lieu and Lockman 1998) and A2199 clusters (Lieu, Bonamente and Mittaz 1999). Recent attributions of these findings to spatial variations of the background (Bowyer, Berghoefer and Korpela 1999) were based upon an incorrect way of analyzing the EUVE data, and the decisive way of assessing the existence of CSE emission is that of an *in situ* background measurement by pointing time contiguously at small offsets from the cluster. This approach, applied to a recent EUVE re-observation of A2199 (Lieu et al. 1999b), clearly demonstrated that the offset pointing provides an accurate background template for the cluster observation, whereas an arbitrary blank field does not. With the aid of the new data, we were able to confirm the previous detection of CSE even in the most conservative case when we assumed no *a priori* understanding of the background distribution, so that a point-to-point subtraction of the background had to be adopted.

Recently, EUVE re-observations of A1795 and Virgo were performed along with acquisition of *in situ* background. We provide in this analysis two ways of utilizing the background data, one is to develop a model of the background and the other is direct subtraction of the offset field as in the case of A2199.

2 Virgo

A 46 ks EUVE observation of the Virgo cluster took place in February 1999, featuring a 34 ks pointing to the central galaxy M87 *immediately* followed by a 12 ks pointing at $\sim$ 2 degrees offset and with the same celestial orientation of the Lex/B filter. This observational strategy (see Lieu et al. 1999b for details) revealed the obvious detection of a halo of EUV emission around M87 of radius $\sim$ 15 arcmin (Fig.1, top), confirming the original discovery (Lieu et al. 1996a). For both source and offset fields only the central, mildly vignetted parts of the DS Lex/B filter were considered (events with Y detector coordinate in the $\sim$ 850-1200 range[a], see Lieu et al. 1999c). The *in situ* background measurement (Fig. 1, bottom) with the center of the annuli placed at the same detector position as that of the cluster's radial profile, indicates a distribution of surface brightness consistent with uniformity: the percentage deviation between the region occupied by the cluster and that beyond is statistically insignificant (the difference between the count rate of the 0–17$'$ and 17–27$'$ regions is 0.8$\pm$1.2 %).

To account for any trends in the background radial profile which may be masked by statistical fluctuations of the measured data, we utilize the well established fact that the background consists of a spatially uniform particle component and a photon component which is vignetted (see section 4.2 and Figure 7 of Sirk et al. 1997). Although the precise relative proportion varies with time, the former usually dominates, resulting in a radial profile which is flat or slowly varying with no change in behavior at any particular radius, small scale ripples in the profile are negligible (Lieu et al 1999c). Thus an empirical model of the background which involves a linear slope was satisfactorily fitted to the radial profile data at arcmin resolution, the slope and intercept and their uncertainties were used to compute the background and its error at any radius with the same resolution, as demonstrated in Figure 2.

This model is then subtracted from the cluster data with propagation of errors. Such a procedure was adopted, along with our constraints on the hot ICM parameters (see below), to obtain the radial trend of the fractional EUV excess, the dashed diamonds in Figure 3. For the more cautious reader, however, we also provided in Figure 3 (dotted diamonds) the fractional EUV excess profile obtained from point-to-point subtraction of the *in situ* background and proper error propagation, when the subtraction was done after scaling away a small difference ($\sim$ 0.3%) in the absolute background level between the cluster and offset fields, by normalizing the 17 – 27 arcmin brightness of the two pointings (see Figure 1). The small difference between the aforementioned background levels gives further indication that a contemporaneous, *in situ* offset pointing affords the most relevant background measurement (background levels in the DS detector have a dynamical range of $\sim$ 300 % thoroughout the entire mission). It can be seen that even this approach, which yields the most conservative estimates of the soft excess, indicates positive signals and a rising radial trend. In fact, the two background subtraction procedures gave statistically consistent results at all radii.

[a]The mildly vignetted portion of the detector Y axis covers a linear size of $\sim$ 26 arcmin; this implies that for radii $\geq\sim$ 13 arcmin the radial profiles are averaged only over those azimuthal angles that fall within the given Y axis detector limits.

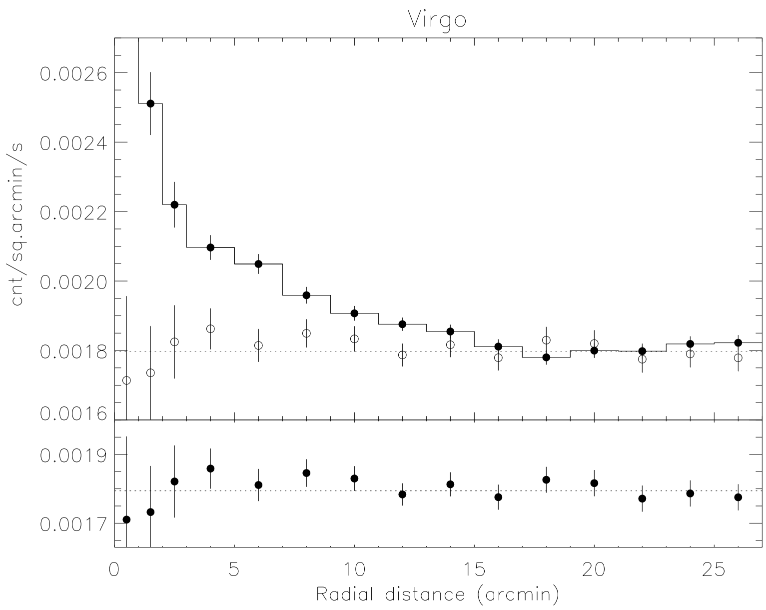

Figure 1: Radial profile of the cluster pointing (top) and offset pointing (bottom) of the Virgo observation. For both plots the radius is measured from the detector position of M87. The innermost 1' bin of the cluster, dominated by the emission from M87, is omitted. Both profiles are plotted in the same scale. The dotted line represents average brightness of the 17'–27' region. On same ordinate of the cluster pointing (top) is overplotted the radial profile of the offset pointing with open circles, after a ~ 0.3 % rescaling (the difference between the 17'–27' region brightness of the two profiles) is applied.

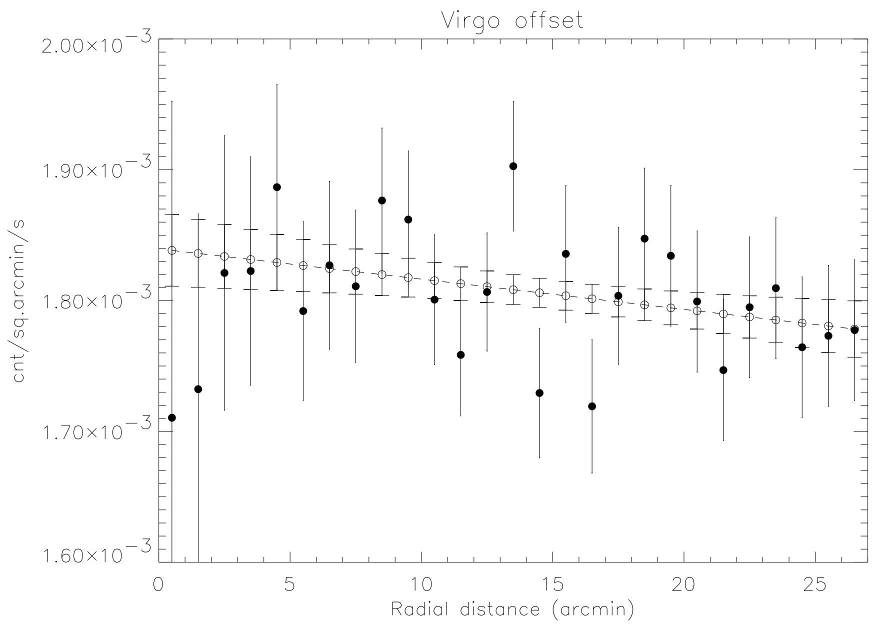

Figure 2: Best-fit linear slope (dotted line and open circles), with relative errors, to the Virgo offest radial profile (solid circles) at 1' resolution.

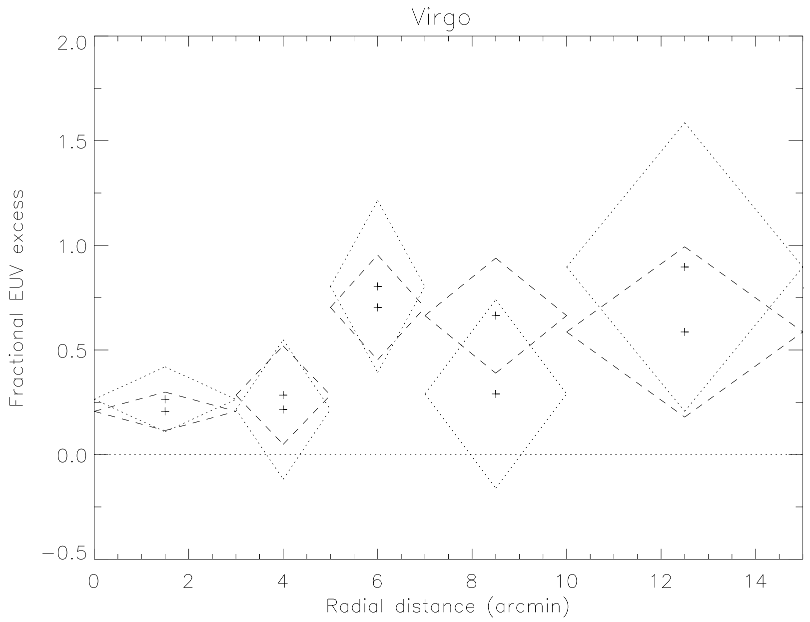

Figure 3: Radial profile of the EUV fractional excess η of Virgo, defined as $\eta = (p - q)/q$, where p is the observed EUV band flux after background subtraction, and q is the expected flux from the hot ICM. Vertical semi-diameters are here and after 1-σ errors. Dashed diamonds are obtained by subtraction of model background, dotted diamonds by point to point background subtraction.

In order to provide an accurate model of the hot ICM and its emissivity in the EUV band[b], an archival ROSAT PSPC observation of the Virgo cluster (RP number 800365) was analyzed. Here, effects of the gradient of Galactic line-of-sight HI column density (N_H) over the Virgo region, which are not entirely negligible, need to be evaluated. The N_H was shown by a recent 21 cm measurement (Lieu et al. 1996a) to radially increase from $\mathrm{N}_H = 1.8 \times 10^{20}$ cm^{-2} at the cluster center to $\mathrm{N}_H = 2.0 \times 10^{20}$ cm^{-2} at the radius interval of 15 – 19 arcmin. This was confirmed by IRAS 100 μm images (Wheelock et al. 1994; Snowden 2000), and we consequently applied a higher N_H value to the outer regions of Virgo when modelling the spectral data. Given the radial HI variation (which continues its rising trend beyond 19 arcmin), and the known anti-correlation between HI and the 1/4 keV diffuse sky background (Snowden et al. 1998), one must assess how much the PSPC background was underestimated for the cluster region when it was determined, as in our case, from a $\sim$ 40–50 arcmin annulus centered at M87. Of most concern is the 10–15 arcmin annulus, where the 1/4 keV sky background accounts for 12% of the detected flux in this band. A re–scaling of this background in accordance with the HI gradient (Snowden et al. 1998) over the annulus only leads to a negligible effect on the 1/4 keV excess (viz. a reduction by 1% from our reported precentage excess, see below).

The emission from the hot ICM is at sufficiently low temperature (1–3 keV) to enable a spatially resolved temperature determination with PSPC data. PSPC R27 band X–ray spectra (PI channels 20–201, $\sim$ 0.2–2.0 keV by photon energy; Snowden et al. 1994) were modelled, using the XSPEC software, with a photoelectrically absorbed single temperature MEKAL code (Mewe, Gronenschild and Van den Oord 1985; Mewe, Lemen and van den Oord 1986; Kaastra

[b]The PSPC data used in this paper were reduced according to the prescriptions of Snowden et al. (1994) through the use of dedicated FTOOLS such as PCPICOR and PCARF, which correct for detector gain changes and sensitivity variations over the PSPC field of view. Background fluxes are estimated from an outer annular region (near $\sim$ 45 arcmin from PSPC boresight) where the cluster contribution is considered negligible. Periods of high background (MV ratio $\geq$ 170) were also rejected and PI channels 1–19 and 202–256, which suffer from calibration uncertainties, were not used.

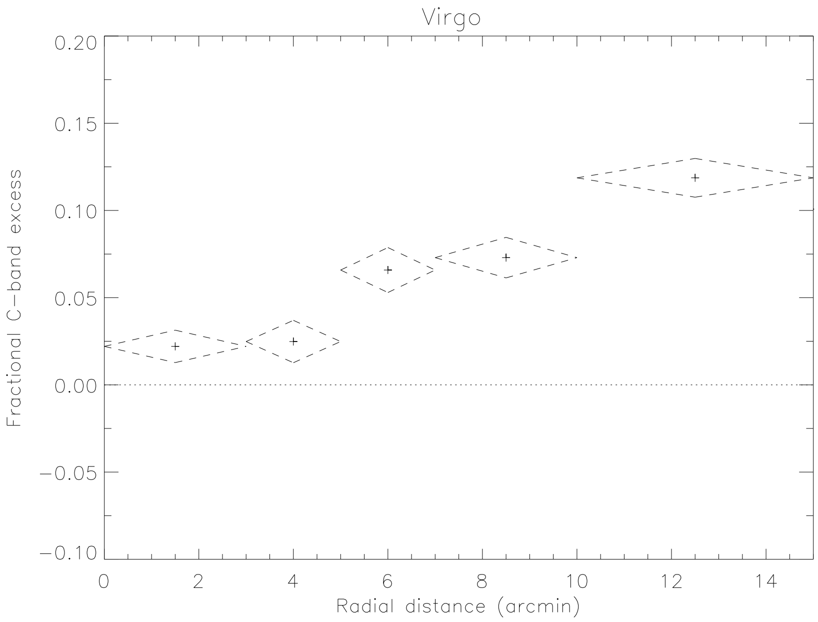

Figure 4: Radial profile of the C-band fractional excess η of Virgo.

1992), and the temperature and elemental abundances were fitted to the data. By means of the hot ICM parameters we assessed the existence of soft–excess in the EUV measurements. The results, as shown Figure 3, are positive. Further, they indicate the soft excess radial trend (SERT), or more precisely an increase in the fractional excess with radius. It should be mentioned that significant soft excess is also apparent in the C-band (synonimous with R2, see Snowden et al. 1994) as single temperature models do not fit well the PSPC data (Figure 4; see also Lieu et al 1996a, Buote 2000).

3 A1795

A1795 was recently observed by EUVE for $\sim$ 78 ks of exposure. The observational strategy utilizes the elongation of the DS Lexan/B filter (see, e.g., Figure 7 of Sirk et al. 1997). For about half of the observation, cluster emission was collected on one side of the detector, leaving the other side exposed only to background counts. For the remaining half of the time the role of the two sides was exchanged. Since our calculations based on the detected cluster EUV flux indicate that cluster's presence on the far side has no effect on the asymptotic background, this technique affords a time contiguous measurement of the cluster signals and the *in situ* background with equal exposures. The background radial profile was again found to be consistent with uniformity, as shown in Fig. 5, where the difference between the average count rate of the 2–11$'$ and 11–23$'$ regions is 1.05 $\pm$ 0.97 %. The CSE effect was detected out to a radial distance of $\sim$ 10 arcmin from the center, confirming the previous EUVE observation (Mittaz, Lieu and Lockman 1998). The two possible procedures of determining and subtracting this background, adopted below to obtain statistically consistent fractional EUV excess profiles, were already described in section 2.

Two archival ROSAT PSPC observations (RP numbers 800055 and 800105) were analyzed, to constrain the hot ICM parameters. The line-of-sight HI is smoothly distributed at $N_H = 1.05 \times 10^{20}$ cm^{-2} in the direction of A1795 (Mittaz, Lieu and Lockman 1998), and the R27 band spectra of annular regions were fitted with a MEKAL model, the abundance being fixed at 0.31 solar (Fabian et al 1994). The resulting EUV excess emission is shown in Figure 6; like Virgo,

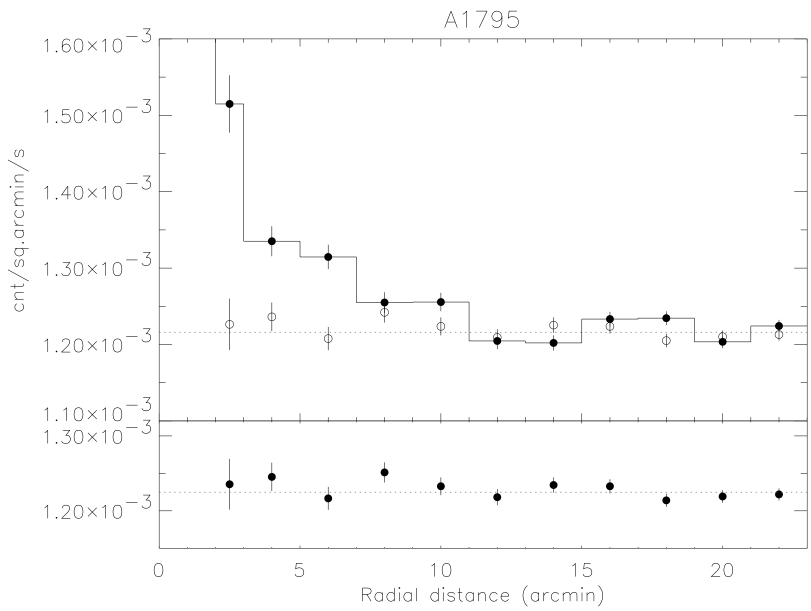

Figure 5: Radial profile of the co-added cluster pointings (top) and offset pointings (bottom) of the A1795 observation. The innermost 2' bins are omitted, as there was substantial contamination from a bright unidentified transient source near the cluster center. On either plot the dotted line represents average brightness of the 11'–23' region. There is no statistically significant deviation of the background profile from that of a uniform distribution: difference between the average levels for the 2'–11' and 11'–23' annuli is 1.05 $\pm$ 0.97 %. On same ordinate of the cluster pointing (top) is overplotted the radial profile of the offset pointing with open circles, after a $\sim$ 0.7 % rescaling (the difference between the 11'–23' region brightness of the two profiles) is applied.

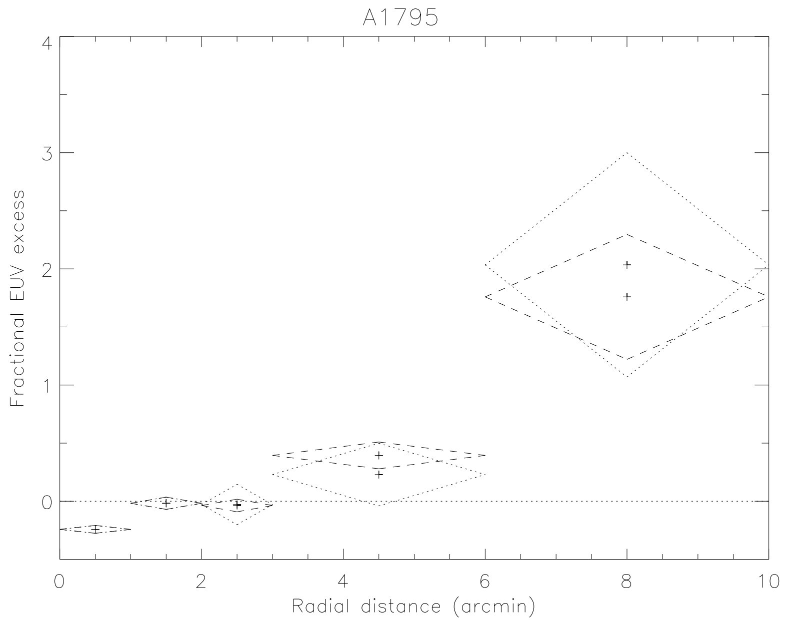

Figure 6: Radial profile of the EUV fractional excess η for A1795. Owing to contamination from a transient source (see Figure 5), data for the 0–2 arcmin bins are from a previous observation of the cluster (Mittaz, Lieu and Lockman 1998). Note also that this previous paper showed a similar plot with a stronger rising trend, because it used absorption code of Balucinska-Church and McCammon (1992), whereas the present work uses the original Morrison & McCammon (1982) code, which is now believed to involve a more reliable He cross-section (see text). Dashed diamonds are obtained by subtraction of model background, dotted diamonds by point to point background subtraction.

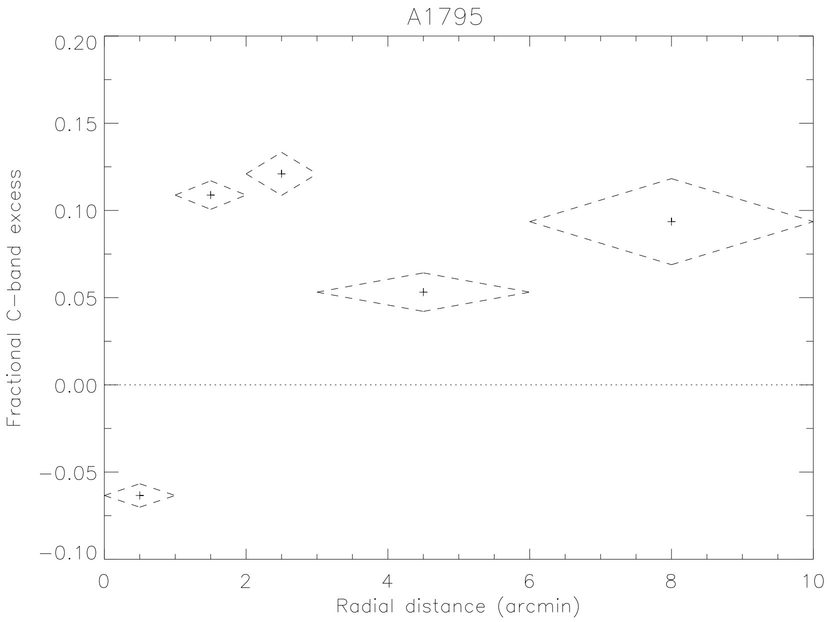

Figure 7: Radial profile of C-band fractional excess of A1795.

it exhibits the SERT effect. We also found existence of CSE in the C-band, see Figure 7.

4 Photoelectric absorption issues

Throughout the analyses of this paper, we employed the absorption cross-sections of Morrison and McCammon (1982; MM82), whose He photoelectric cross-section is in good agreement with the compilation of Yan et al. (1998; Y98), the latter was employed in a recent investigation of the CSE (Arabadjis and Bregman 1999). In the C-band the MM82 and Y98 He cross-sections differ by $\sim 1\%$, whereas in the Lex/B passband ($\sim$ 65-190 eV) the Y98 cross-section is actually *lower* than in MM82 by $\sim$8 %, i.e. the new cross-section renders our CSE fluxes even more prominent. Given that the cross section is not an issue, the proposition that the CSE detection of some clusters (including A1795 and Virgo) is in some way related to peculiarities in the Galactic absorption faces two problems. Firstly, the N_H values needed to remove the CSE are grossly at odds with the ones measured by the dedicated observations of Mittaz, Lieu, & Lockman (1998). For example, we found that the spectrum of the $7 - 10$ arcmin annulus of Virgo can satisfactorily be fitted by a one temperature plasma model (with *no* soft component) only by adopting an N_H as low as $1.34 \pm 0.07 \times 10^{20}$ cm^{-2}. Secondly the SERT effect (e.g., Fig. 3 and Fig. 6) implies a curious spatial correlation between our Galactic interstellar medium and the centers of the two clusters. We therefore conclude that the CSE is a genuinely celestial emission component.

5 Interpretation of the *soft* component and conclusions

We now discuss the physical significance of the soft component. Currently there are two contesting models: the non–thermal scenario, which invokes an Inverse Compton (IC) effect as cause for the emission (Sarazin and Lieu, 1998; Hwang 1997; Ensslin and Biermann 1998), and the original thermal model, which explains the CSE as thermal emission from a 'warm' gas ($\sim 10^6$ K; Lieu et al. 1996a).

A recent study of the Coma cluster (Lieu at al. 1999a) showed that the CSE emission could be explained as an IC effect, albeit invoking a large population of energetic electrons. When the present Virgo soft excess was fitted with a power-law, we also accomodated the possibility of 'aging' due to loss of the relativistic electrons to the ICM. [c] Even so, the fit was far from acceptable. A simple power-law model for the soft component requires an extremely large value of the differential photon number index (Table 1), inconsistent with the value of $\sim$ 1.75-2 expected from a population of electrons accelerated at astrophysical shocks (see Lieu et al. 1999a and references therein). When aging effects are included, a satisfactory fit can be found only for some of the regions, and the model was rejected for regions of strongest signal (0-7$'$ from M87; see Table 1). The CSE can be explained, however, as thermal emission from a thin plasma at lower temperature ($\sim$ 0.1 keV, see Table 1), following the original interpretation of Lieu et al. (1996a).

Table 1: Modelling of Virgo spectra with a two–temperature MEKAL code (left), MEKAL + power-law model (center) and MEKAL + 'aged' power-law model (right). Errors are 90 % confidence (χ^2 + 2.701 criterion). For the latter, the IC magnetic field was fixed at 1μG, the density of the ICM calculated from the best-fit β-model of Nulsen and Böhringer (1995) and the electron differential number index γ fixed at the value of 2.5 (wich corresponds to a similar photon index α of 1.75). The parameters of the hot phase were fixed at those best values obtained by fitting PI channels 42 – 201 with a single temperature model of floating abundance. N_{warm} is here and after in units of $10^{-14}/4\pi D^2 n^2 V$, where D (cm) is the distance to the source, n (cm^{-3}) is the gas density and V (cm^3) is the volume of the emitting region.

	MEKAL+MEKAL			MEKAL+PO		MEKAL+'aged' PO	
Region (arcmin)	T_{warm} (keV)	N_{warm} $\times 10^2$	red. χ^2(d.o.f.)	α	red. χ^2(d.o.f.)	t_{age} (Gyrs)	red. $\chi^2(d.o.f.)$
0–3	$0.066 \pm^{0.038}_{0.014}$	$0.36 \pm^{0.24}_{0.16}$	1.18(181)	$3.3 \pm^{2.4}_{0.6}$	1.15(181)	~ 0	1.6(181)
3–5	$0.079 \pm^{0.039}_{0.016}$	$0.28 \pm^{0.07}_{0.08}$	1.2(181)	$4 \pm^{1.4}_{0.6}$	1.2(181)	~ 0	1.66(181)
5–7	$0.079 \pm^{0.022}_{0.015}$	$0.4 \pm^{0.2}_{0.12}$	1.28(180)	$4.4 \pm^{1.2}_{0.7}$	1.24(180)	~ 1.1	2(180)
7–10	$0.09 \pm^{0.01}_{0.012}$	$0.59 \pm^{0.25}_{0.13}$	1.28(180)	$4.2\pm^{0.8}_{0.5}$	1.24(180)	$1.8\pm^{0.015}_{0.02}$	1.11(180)
10–15	$0.083 \pm^{0.009}_{0.011}$	$1.1 \pm^{0.38}_{0.1}$	1.3(180)	$4.5\pm^{0.65}_{0.3}$	1.27(180)	$2.1\pm^{0.15}_{0.05}$	1.2(180)

Table 2: Modelling of A1795 spectra with a two-temperature MEKAL code (left) and with a MEKAL + 'aged' power-law code (right); errors are 90% confidence (χ^2 + 2.701 criterion). Parameters of the hot phase were fixed at those best values obtained by fitting PI channels 42 – 201 with a single temperature model of abundance 0.31 solar (Fabian et al 1994). For the non-thermal model, the value of the IC magnetic field was fixed at 1μG; the density of the ICM, a parameter which affects the aging of electrons, was calculated from the best-fit β-model of Briel and Henry (1996). Electron differential index γ was fixed at the value of 2.5 (see Table 1).

	MEKAL+MEKAL			MEKAL+'aged' PO	
Region (arcmin)	T_{warm} (keV)	N_{warm} $\times 10^2$	red. χ^2 (d.o.f)	t_{age} (Gyrs)	Red. χ^2(d.o.f)
1–2	$0.125\pm^{0.034}_{0.037}$	$0.045\pm^{0.008}_{0.009}$	1.0(363)	$1.7 \pm^{0.17}_{0.11}$	1.0(363)
2–3	$0.11\pm^{0.04}_{0.02}$	$0.0285\pm^{0.006}_{0.007}$	1.16(363)	$2.25 \pm^{0.15}_{0.55}$	1.15(363)
3–6	$0.049\pm^{0.017}_{0.015}$	$0.12\pm^{0.37}_{0.06}$	0.97(363)	$2.8 \pm^{0.1}_{0.13}$	0.98(363)
6–10	$0.025\pm^{0.013}_{0.012}$	$110\pm^{700}_{70}$	0.88(363)	$3.7 \pm^{0.16}_{0.14}$	0.88(363)

Fitting of the CSE of A1795 with a non-thermal model produced a similar outcome. At large radii, the EUV excess is accompanied by a weaker C–band excess. This necessitates a sharp cut–off, which can be understood as due to aging, and a highly evolved IC spectrum is a

[c] A spectral code which introduces radiative (synchrotron and IC) and non–radiative (Coulomb) losses on a power–law model was integrated with the XSPEC spectral fitting package. As function of 'aging' time (t_{age}) and environmental conditions (such as density of the hot gas and magnetic field strength), electrons at all energies are progressively removed, modifying the resulting emissivity.

possible model, Table 2. However, the energetic requirements are severe, see Table 3, because the electron pressure alone (in the absence of relativistic ions, which accentuates the difficulty $\sim$ 10 - 100 times) often exceeds that of the hot ICM. The 6–10 arcmin region requires relativistic electrons which, at time of injection, had a pressure $\sim$ *four times higher* than that of the hot gas, leading to major confinement problems. The thermal scenario again appears more appropriate: the data of Table 2 indicate that a $\sim$ 0.05–0.1 keV gas can satisfactorily explain the CSE.

Table 3: Luminosity and pressure estimates for A1795; L_{42}^{CSE} is the intrinsic luminosity of non–thermal best–fit model between photon energies 65–250 eV (γ_{min}=279 and γ_{max}=548) in units of 10^{42} (erg s^{-1}) and P^{CSE} is the pressure of relativistic electrons in the [γ_{min},γ_{max}] Lorentz factor interval. P^e and $P^e(t=0)$ are the total electron pressure at the present epoch and at the acceleration epoch, respectively, assuming cosmological parameters $H_0 = 75$ km s^{-1} Mpc^{-1} and $q_0 = 0$. If $H_0 = 50$ km s^{-1} Mpc^{-1} is adopted, all present pressure estimates for the non-thermal component will increase $\sim$ two-fold. Pressure for the ICM (P^{gas}) was calculated according to the parameters of Briel and Henry (1996).

Region (arcmin)	L_{42}^{CSE}	P^{CSE} (erg cm^{-3})	P^{gas}/P^{CSE}	P^{gas}/P^e	$P^{gas}/P^e(t=0)$
1–2	0.9	1.6 10^{-13}	88.3	35.3	1.9
2–3	1.3	1.0 10^{-13}	128	85.8	4.8
3–6	4.5	1.0 10^{-13}	120	52.7	2.3
6–10	22.0	6.8 10^{-14}	17.6	2.5	0.22

Table 4: Warm gas mass estimates and comparison with the hot ICM for the Virgo and A1795 cluster (see Tables 1 and 2). Warm gas densities (n_{warm}) are estimated for 100% filling factors.

	Virgo			A1795	
Region (arcmin)	n_{warm} (10^{-3} cm^{-3})	n_{hot} (10^{-3} cm^{-3})	Region (arcmin)	n_{warm} (10^{-3} cm^{-3})	n_{hot} (10^{-3} cm^{-3})
0–3	$5.2 \pm^{3.4}_{2.4}$	50	0–1	—	3.7
3–5	$2.4 \pm^{0.6}_{0.65}$	10	1–2	$0.92\pm^{0.16}_{0.18}$	3.3
5–7	$1.9 \pm^{1}_{0.6}$	7.5	2–3	$0.45\pm^{0.1}_{0.11}$	2.7
7–10	$1.4 \pm^{0.6}_{0.3}$	5	3–6	$0.3\pm^{0.9}_{0.15}$	1.6
10–15	$1.0\pm^{0.34}_{0.1}$	3	6–10	$4.5\pm^{26}_{2.6}$	0.93

What are, then, the implications of the thermal interpretation on cluster masses? In absence of any knowledge on the clumping of the warm phase, a 100 % filling factor implies a warm gas mass comparable with that of the hot gas (Table 4). This is in good overall agreement with recent large–scale hydrodynamical simulations (Cen and Ostriker 1999) which indicate that at the present epoch the baryons are to be found, in similar amounts, at hot ($\sim 10^8$ K) and warm ($\sim 10^5 - 10^7$ K) temperatures, and only marginally at lower temperatures (see also Bonamente, Lieu and Mittaz 2000 for the detection of cold clouds with commensurately smaller mass budgets).

References

1. J.S. Arabadjis and J.N. Bregman, *ApJ* **514**, 607 (1999).
2. M. Baluchinska-Church and D. McCammon , *ApJ* **400**, 699 (1992).
3. M. Bonamente, R. Lieu and J.P.D. Mittaz, *ApJ* **in press**, (2000).
4. S. Bowyer and R.F. Malina , *EUV Astronomy, eds. R.F. Malina and S. Bowyer (New York:Pergamon)* , 397 (1991).

5. S. Bowyer, T. Berghöfer and E. Korpela, *ApJ* **526**, 592 (1999).
6. U.G. Briel and J.P. Henry, *ApJ* **472**, 131 (1996).
7. D.A. Buote, *ApJ in press* , (2000).
8. R. Cen and J.P. Ostriker, *ApJ* **514**, 1 (1999).
9. T.A. Ensslin and P.L. Biermann, A&A **330**, 90 (1998).
10. A.C. Fabian, K.A. Arnaud, M.W. Bautz and Y. Tawara, *ApJ* **436**, L63 (1994).
11. C.-Y. Hwang, *Science* **278**, 1917 (1997).
12. J.S. Kaastra,*An X-Ray Spectral Code for Optically Thin Plasmas, Internal SRON-Leiden Report, updated version 2.0* , (1992).
13. R. Lieu, J.P.D. Mittaz, S. Bowyer, F.J. Lockman, C.-Y. Hwang and J.H.H.M. Schmitt 1996a, *ApJ* **458**, L5 (1996a).
14. R. Lieu, J.P.D. Mittaz, S. Bowyer, J.O. Breen, F.J. Lockman, E.M. Murphy and C.-Y. Hwang,1996b, *Science* **274**, 1335 (1996b).
15. R. Lieu, W.-I. Ip, W.I. Axford and M. Bonamente, *ApJ* **510**, L25 (1999a).
16. R. Lieu, M. Bonamente, J.P.D. Mittaz, F. Durret, S. Dos Santos and J.S. Kaastra, 1999, *ApJ* **527**, L77 (1999b)
17. R. Lieu, M. Bonamente, J.P.D. Mittaz, F. Durret, S. Dos Santos *Proceedings of the Workshop on 'Diffuse Thermal and Relativistic Plasma in Galaxy Clusters, Ringberg, Germany MPE report 271* , 197 (1999c).
18. R. Mewe, E.H.B.M. Gronenschild, and G.H.J. van den Oord, *A&A Supp.* **62**, 197 (1985).
19. R. Mewe, J.R. Lemen, and G.H.J. van den Oord, *A&A Supp.* **65**, 511 (1986).
20. J.P.D. Mittaz, R. Lieu, F.J. Lockman, *ApJ* **498**, L17 (1998).
21. R. Morrison and D. McCammon, *ApJ* **270**, 119 (1983).
22. P.E.J. Nulsen and H. Böhringer, *MNRAS* **274**, 1093 (1995).
23. C.L. Sarazin and R. Lieu, *ApJ* **494**, L177 (1998).
24. M.M Sirk, J.V. Vallerga, D.S. Finley, P. Jelinsky and R.F. Malina, *ApJS* **110**, 347 (1997).
25. S.L. Snowden, R. Egger, D.P Finkbeiner, M.J. Freyberg and P.P. Plucinsky, *ApJ* **493**, 715 (1998).
26. S.L. Snowden, in preparation , (2000).
27. Weelock et al.,*IRAS Sky Survey Explanatory Supplement (JPL Publication 94-11), Pasadena, CA* , (1994).
28. M. Yan, H.R. Sadeghpour and A. Dalgarno, *ApJ* **496**, 1044 (1998).